Journal of Materials Science and Engineering with Advanced Technology
Volume 14, Number 2, 2016, Pages 47-68
Available at http://scientificadvances.co.in
DOI: http://dx.doi.org/10.18642/jmseat_7100121730

DIFFUSE PHASE TRANSITION AND IMPEDANCE SPECTROSCOPY ANALYSIS OF $Sr_2KNb_5O_{15}$ FERROELECTRIC CERAMIC

A. NEQALI[1], E. CHOUKRI[1], A. BELBOUKHARI[1], Z. ABKHAR[1], Y. GAGOU[2], L. HAJJI[1], M. EL MARSSI[2], A. NAJMEDDINE[3] and D. MEZZANE[1]

[1]LMCN
F.S.T.G. University Cadi Ayyad Marrakech
Morocco
e-mail: Aziz.neqali@gmail.com

[2]LPMC
Université de Picardie
33, rue Saint-Leu
80039 Amiens Cédex
France

[3]LMF
Faculté des Sciences de Sfax
BP 1171, 3000 Sfax
Tunisie

Abstract

In this work, we study the sample $Sr_2KNb_5O_{15}$ prepared using conventional solid state synthesis under air. X-ray analysis shows that it is a single-phase TTB structure. Impedance spectroscopy analysis of the dielectric properties of $Sr_2KNb_5O_{15}$ ceramics were investigated in the frequency range, 10Hz-1MHz

Keywords and phrases: TTB, ferroelectrics, dielectric, impedance, conductivity.
Received October 8, 2016

and in the temperature region from ambient temperature to 350°C. Impedance and conductivity plots were used to analyze the sample behaviour versus frequency. Cole–Cole plots showed non-Debye relaxation. The nature of variation of the electrical conductivity, and the activation energy value for different temperature ranges, indicate that the conduction process is of mixed-type (i.e., ionic polaronic and space charge generated from the oxygen ion vacancies). Analysis results of dielectric properties will be compared to three compounds of TTB structure that are derived from SKN compound family: $Pb_{0.75}K_{0.5}Nb_2O_6$ (PKN) in which the Pb is substituted by Sr, $K_3Li_2Nb_5O_{15}$ (KLN) in which the Li is substituted by Sr, and $Pb_{1.8}Gd_{0.1}K_{1.1}Nb_5O_{15}$ (PKGN) in which the Pb and Gd are substituted by Sr.

1. Introduction

Considerable attention has been given to the study of niobates of tetragonal tungsten bronze type ferroelectrics (TTB) in the last few years. This structure is one of the greatest and yet purely studied families of ferroelectric oxides. They are described as a framework of MO_6 octahedra (M = metal of transition, in our case M = Nb) sharing corners, which reveals three kinds of tunnels with pentagonal (*p*), square (*c*), and triangular (*t*) sections [1, 2]. The first two sites of coordination number, respectively, 15 and 12 can be occupied by ions of large size while the third one, of coordination number 9, can only be occupied by small size ions [3, 4].

Deep studies of some ferroelectric materials of the TTB structural family exhibit the occurrence of high electric permittivity (ε) and low dielectric loss [5, 6] as well as interesting ferroelectric, pyroelectric, piezoelectric, and nonlinear optical properties. All these properties are useful for various devices such as transducers, actuators, capacitors, and ferroelectric random access memory devices [7, 8]. Ionic substitutions in TTB structures play an important role in improving their physical properties [8, 9].

This paper aims the dielectric and structural properties of solid state synthesized $Sr_2KNb_5O_{15}$ (SKN) ceramics. The X-ray diffraction shows the orthorhombic phase with the space group P4bm. Dielectric experiments show that the ferroelectric niobate ceramic SKN presents one phase transition at T = 156°C which have been confirmed also by X-ray studies. The origin of frequency dispersion of dielectric constant was analyzed by complex impedance spectroscopy technique. More details of these results and their discussion are presented further.

2. Synthesis, Structure Analysis and Experimental Details

Strontium potassium niobate $[Sr_2KNb_5O_{15}]$ powders were prepared by using the solid state reaction method. First, we mixed K_2CO_3 (chemically pure), SrO_3 (99.99%) and Nb_2O_5 (99.5%). The optimal conditions for the synthesis of the studied composition was determined by series of controlled annealing at different temperatures (1100-1200°C) and holding time (2-12h). The achievement of the single phase compound was confirmed via X-ray diffraction (XRD). The calcined powder was hand ground in mortar agate and pressed into a pellet of 1.3cm in diameter and about 0.1cm in thickness. A load of about 1.5 tons was used to press this pellet. The pressed pellet was heated to 900°C for 2h and finally sintered at 1200°C for 4h in air atmosphere using an alumina crucible. By the means of an electron microscope (Figure 1(b)), we could observe that the grains in the main mass of the ceramic had sizes of 1 to 3μm.

The X-ray measurements were performed by using a Siemens D5000 advanced diffractometer. The room temperature XRD pattern is shown in Figure 1(a). A good agreement of a cooper radiation with $\lambda_{K\alpha 1}$ = 1.5406(0)Å and $\lambda_{K\alpha 2}$ = 1.5444(3)Å was observed between measured and calculated interplanar spacing. Profile adjustment calculation of Bragg reflections using the Fullprof software [10] revealed to be coherent for the orthorhombic structure with the space group P4bm symmetry. The lattice

parameters have been found to be $a = b = 1.253$nm and $c = 0.3882$nm at room temperature. The structure, lattice parameters and volume of SKN compounds and their derived compounds are recapitulated in Table 1. We note change in space group and increase in lattice parameters with substitution of Sr by Li (KLN) and decrease with replacement of Sr by Gd (KGN). This differences can be explained by the ionic size of Li $(r = 0.76\text{Å})$, Gd $(r = 1.02\text{Å})$ compared to that of Sr $(r = 1.18\text{Å})$.

Table 1. Structure and lattice parameter of SKN compound with comparison in those of KLN and KGN

Compound	Space group	**a**(Å)	**b**(Å)	**c**(Å)	**V**(Å^3)
KGN	P4bm	12.422	12.422	3.897	601.33
SKN	P4bm	12.530	12.530	3.882	609.57
KLN	P4bm	12.66	12.66	3.870	661.93

The SEM micrograph of SKN is shown in Figure 1(b). The surface morphology indicates the existence of polycrystalline microstructure comprising good grain growth with shape anisotropy. The grains are homogeneously and uniformly distributed over the entire volume of the sample which means a good crystallization with a certain degree of porosity. The average grain size is $d = 1\text{-}3\mu$m.

To study the electrical properties of the compound, both flat surfaces of the sintered pellets were electroded with air-drying conducting silver paste. Dielectric measurements were carried by using the Solartron SI-1260 spectrometer in the frequency range $10–10^6$ Hz. A source of 1Vrms was applied to the silver electroded pellet ceramic sample having 1mm of thickness. The temperature variation was performed using a Linkam TS 93 hot stage with a temperature stability of ± 0.1K. Platinum electrodes were deposited on the two circular faces of the ceramic to get the capacitor shaped samples.

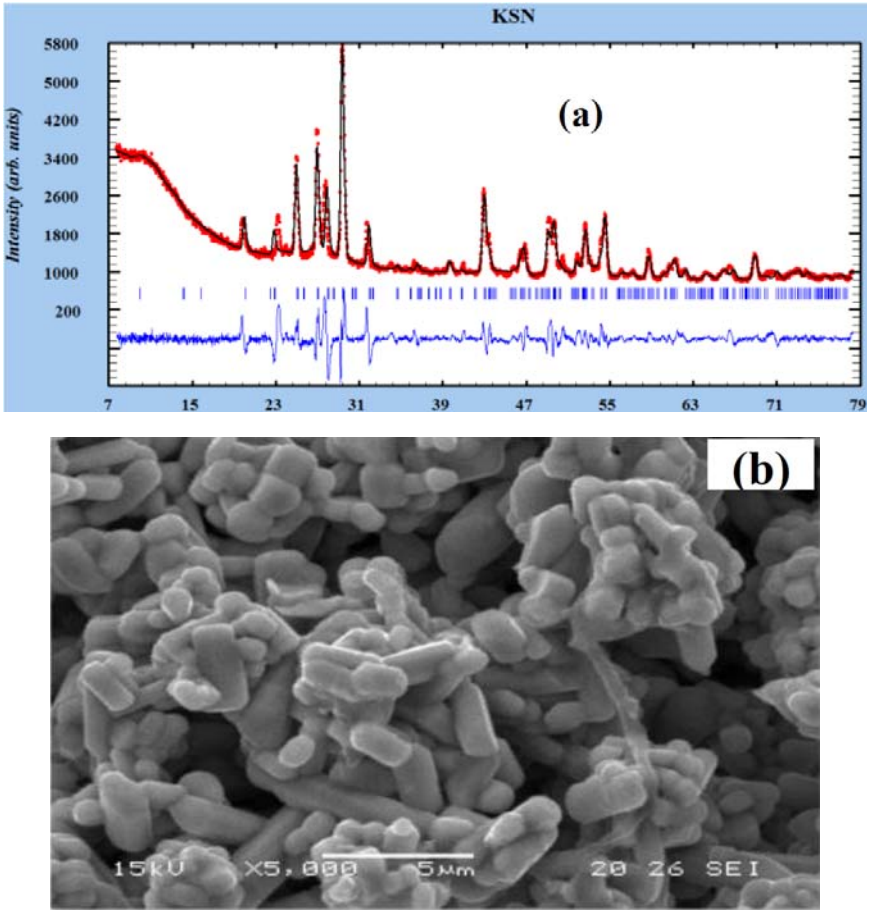

Figure 1. X-ray diffraction patterns of SKN ceramic showing the observed, the calculated, their difference, and Bragg reflections (a); SEM image of SKN (b).

3. Results and Discussion

3.1. Dielectric properties

Figure 2 shows the result of the dielectric measurements for SKN showing the broad maximums ε'_r at T_C = 150°C. The height and the diffuse character of the peak decrease with frequency. The peak position is frequency independent which means that this phenomenon is not

related with relaxor-type behaviour. The observed diffusion is due to the domain walls or topological defects motion in the nucleating ferroelectric phase [11, 12].

The dielectric permittivity at T_C changes as: $\varepsilon'_r(T_C)$ = 2339, 2234, and 1920 at 30, 120, and 300KHz, respectively. At frequencies < 150KHz, the dielectric constant is very high at T_C and keeps decreasing that implies a high concentration of space charge at elevated temperatures [13]. The same behaviour was observed for KGN and KLN ceramics in which the phase transition was masked by the effect of ionic conduction at low frequencies [14, 15].

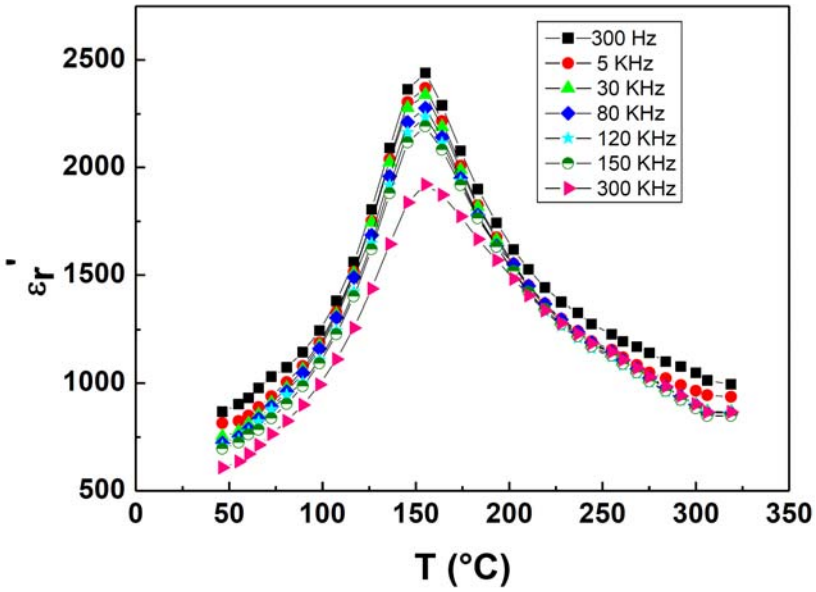

Figure 2. Temperature dependence of the dielectric constant at different frequencies of the ceramic SKN.

Figure 3 shows the inverse of ε'_r versus temperature at different frequencies for the SKN. For $T > T_c$, the curve can be fitted by the linear Curie-Weiss law $\varepsilon'_r = \frac{c}{(T - T_0)}$. Elsewhere and starting from the temperature noted T_b, ε'_r deviates from the Curie-Weiss law. This

deviation from the linear behaviour could be due to the non-uniform distribution of the critical temperatures in the ceramic sample. The following parameters are deduced from the plot: T_C = 150°C, T_0 = 68°C, $C = 1.98 \times 10^5$ K, and $\Delta T = T_b - T_c = 10$°C. The large value of C is a characteristic of oxygen octahedra ferroelectrics [16, 17]. It indicates that the transition is mainly of displacive type [18]. Otherwise, the relatively small value of T_0, compared to the transition temperature T_C, is a characteristic feature of the first-order ferroelectric phase transition [19].

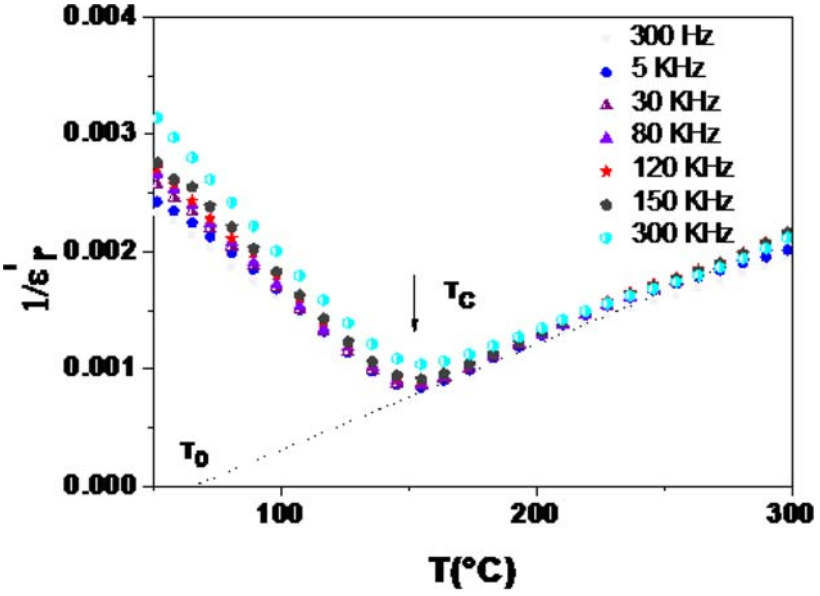

Figure 3. Temperature dependence of inverse susceptibility $1/\varepsilon'_r$ constant at different frequencies of the ceramic SKN.

3.2. Diffusive nature of ferroelectric transition

The diffusive nature of the ferroelectric phase transition can be described respect to Santos-Eiras phenomenological equation [20]:

$$\varepsilon'_r = \frac{\varepsilon'_m}{1 + \left(\frac{T - T_m}{\Delta}\right)^{\gamma}}, \qquad (1)$$

where γ and Δ are assumed to be constants and the γ value is between 1 and 2. The value of γ only depends on the composition of the specimens and gives information on the character of the phase transition (diffuse or not). The experimental results fit, modelled by Equation (1) for $T > T_m$ is shown in Figure 4. The obtained fitting parameters are illustrated in the Table 2. The parameters γ for SKN are found belong to [1.01–1.12]. This leads to the conclusion that DPT in SKN is of "incomplete" nature. This can be related to intrinsic disorder of Strontium sites and/or the distortions of TTB unit cells.

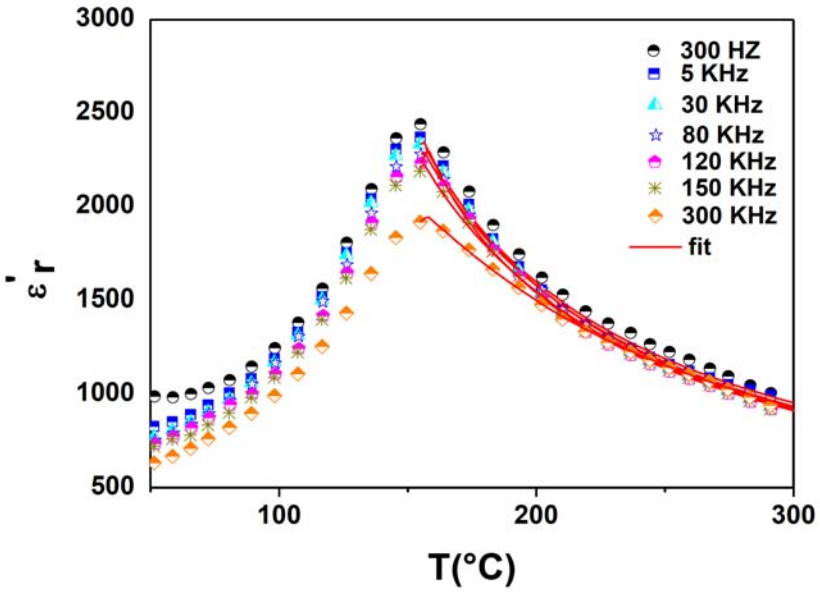

Figure 4. Temperature dependence of ε'_r at different frequencies. Solid lines present the theoretical fit.

Table 2. Dielectric parameters obtained from Santos-Eiras' equation

	300Hz	**5KHz**	**30KHz**	**80KHz**	**120KHz**	**150KHz**	**300KHz**
ε'_m	2480	2399	2367	2298	2262	2225	1943
$T_m(^\circ\mathrm{C})$	156,6	156,36	156,37	156,25	156,58	156,86	157,56
$\Delta(^\circ\mathrm{C})$	856,8	816,3	834,5	842,4	878,7	939,5	126,16
Γ	1,016	1,052	1,05	1,09	1,08	1,05	1,12

3.3. Complex impedance analysis

Variation of the real and imaginary parts of impedance (Z' and Z'') versus frequency within the interval [10Hz-1MHz], for several values of temperature (T = 265°C-325°C), are depicted in Figures 5(a) and 5(b).

It can be seen from Figure 5(a) that, for relatively low frequencies, the Z' magnitudes are large and decrease with the temperature. This is due to the space charge polarization. However, for high frequencies, the Z' magnitudes are no more temperature-dependent and decrease with frequency. This leads to ionic conductivity improvement.

In the other hand, the Figure 5(b) shows that the Z'' magnitudes present peaks that shift toward high frequencies with the temperature, indicating the relaxation time increase and the space charge reduce [21].

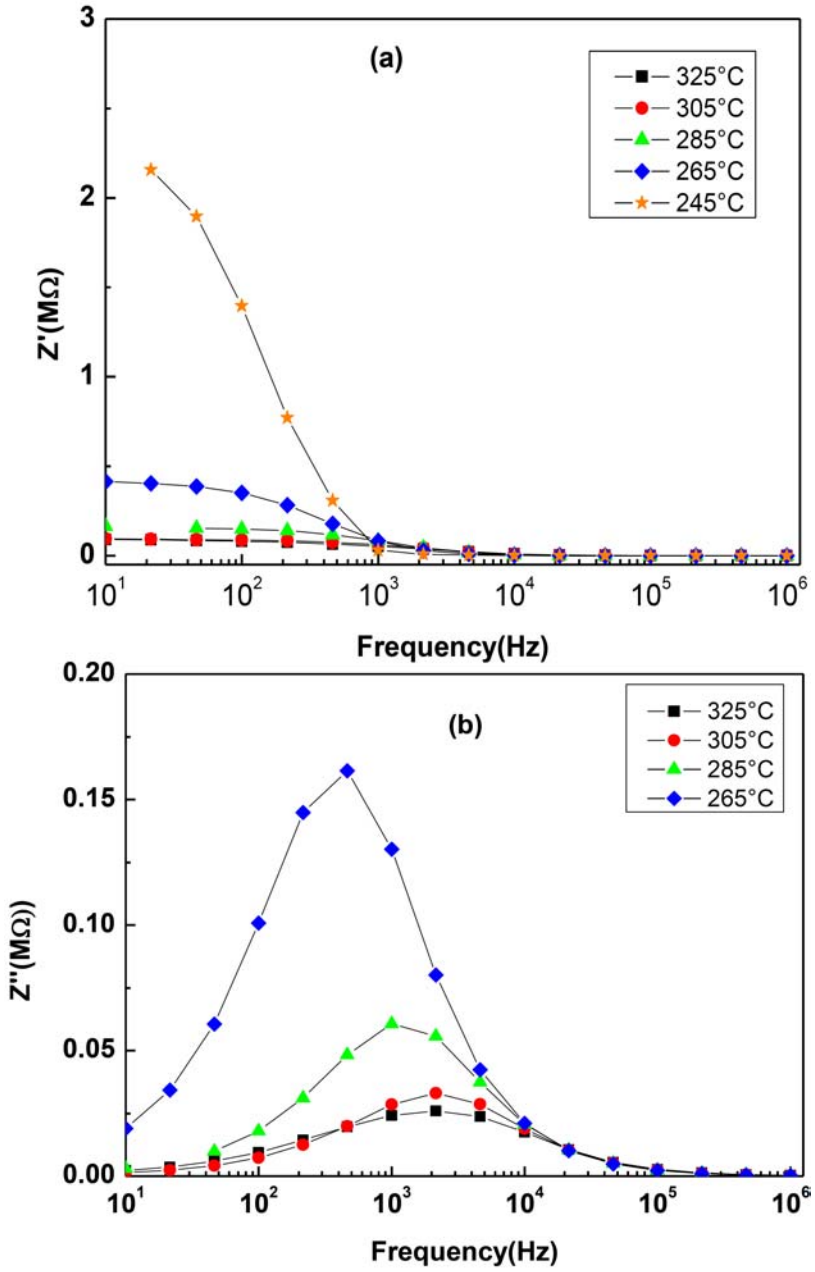

Figure 5. Variation of (a) real (Z') and (b) imaginary ($-Z''$) parts of impedance versus frequency for different temperatures.

Figure 6 gives the normalized imaginary part of the impedance $(Z'' / Z''_{\max})$ as a function of frequency for different temperatures. The curves show asymmetrical peaks, indicating the ionic conductivity relaxation release at high temperatures.

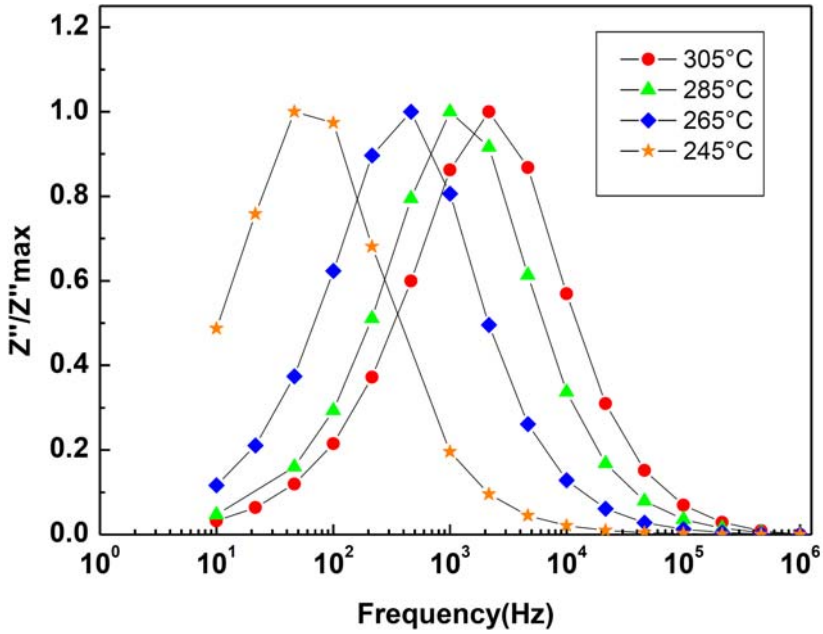

Figure 6. Normalized imaginary parts $Z_i / Z_{i\max}$ of impedance as a function of frequency.

The impedance spectrum analysis is an advantageous means to determine the contribution of grain, grain boundary and electrode to the overall dielectric response of the studied compound. The Nyquist plots (complex impedance spectrum) of SKN at different temperatures are shown in Figure 7. We notice that the semicircles become smaller with temperature and their centers shift towards lower $|Z|$. This means a reduction of grain and grain boundary resistance and negative temperature coefficient of resistance (NTCR) like in semiconductors [22, 23]. The semicircles are not perfect but inclined, and their centers

are placed below the real (Z') axis by an angle $(\alpha - 1)\pi / 2$, where $0 < \alpha < 1$ [24]. This is due to the fact that the relaxation phenomenon is a non- Debye type, because of relaxation time distribution.

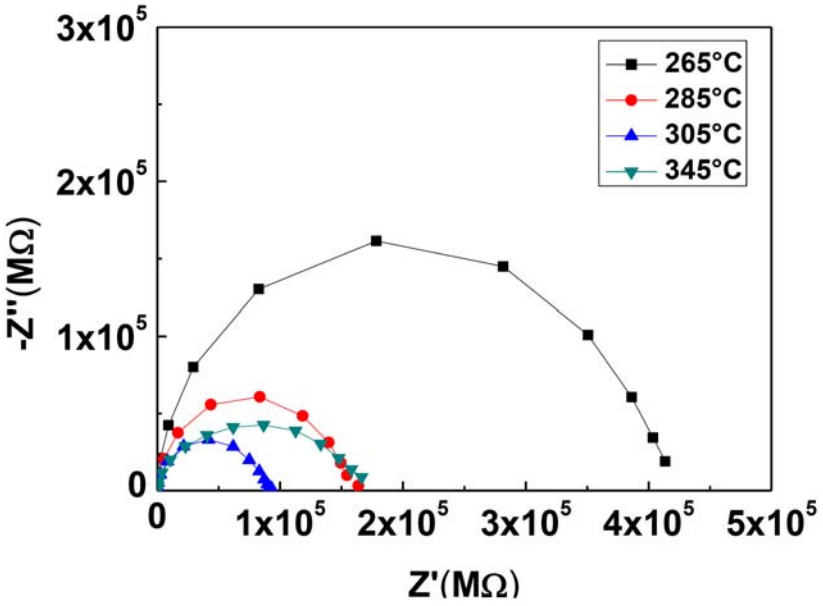

Figure 7. Complex impedance spectrum (Z' vs Z'') of SKN electroceramic.

To model the grains and grain boundaries dielectric properties, the ceramic material can be represented by two parallel RC elements connected in series (Figure 8(a)). The first element models the grain dielectric properties and the second represents the grain boundaries dielectric ones.

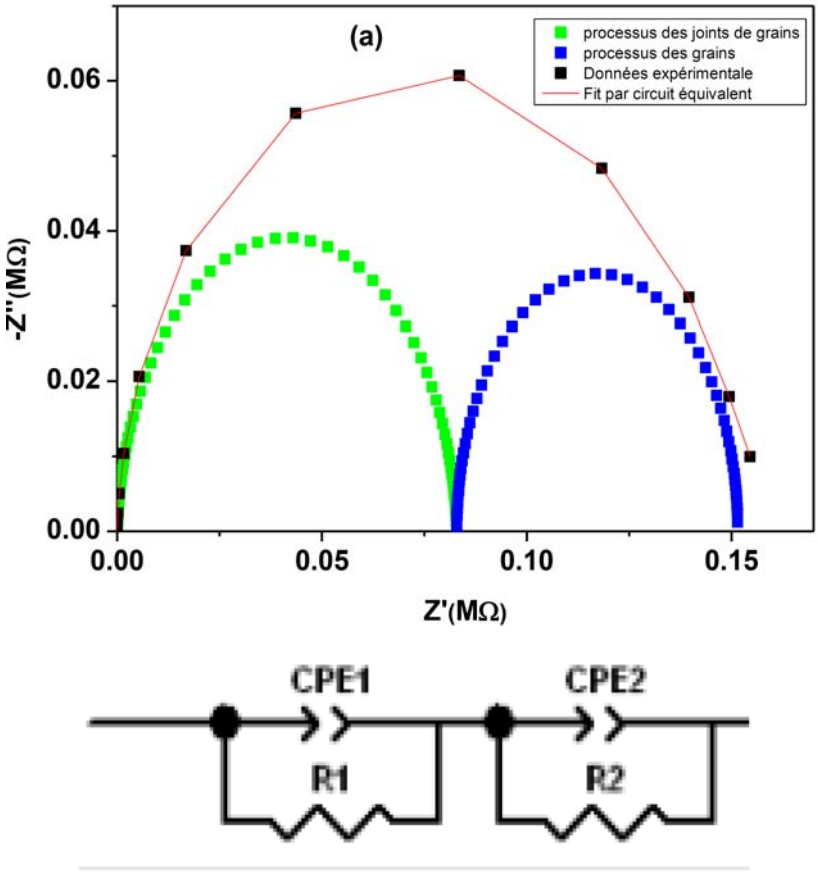

(b)

Figure 8. Complex impedance and deconvoluted plots (a); equivalent circuit used for fitting experiment (b).

The equivalent electrical circuit is presented in Figure 8(b). The impedance of constant phase element (CPE) can be described as [25, 26]: $(CPE) = \frac{1}{T(i\omega)^p}$, where ω is the angular frequency, T and p are constants and $0 < p < 1$. The CPE describes an ideal capacitors with $C = T$ for $p = 1$ and an ideal resistor with $R = 1/T$ for $p = 0$. Therefore, p can be used to represent the degree of perfection of the

capacitor and represents a measure of arc distortion below the real impedance axis. The parameter p is linked to the depression angle as follow: $\alpha_d = (1 - p)\pi^2$.

The complex impedance (Z^*) of each element (CPE//R) is given by:

$$Z(\omega) = \frac{R}{1 + (j\omega\tau)^p}, \tag{2}$$

where $\tau^p = RT$.

The relaxation time constant τ can be described by:

$$\tau = 1 / \omega_{\max} = (RT)^{1/p}. \tag{3}$$

Using the constant phase element (CPE) as shown in Figure 8(a) allows to get a good fit of the experimental data in the whole frequency range. We must note that the modified equivalent RC circuit model using CPE yields to a Argand relaxation type plot. That kind of relaxation is commonly used to study the behaviour of ionic conductors [27]. The resistance R, and the parameters p and T of the CPE were obtained for each temperature. The values of p are found to lie close to unity ($0.95 < p < 0.98$). The constant time τ of grain and grain boundary relaxation were then calculated by using Equation (3). The temperature dependence of the effective grain and grain boundary parameters R_g and R_{gb} in one hand, and of the relaxation times τ_g and τ_{gb} in the other hand, are shown in Figure 9. When temperature increases, the R_{gb} becomes smaller than R_g, which means that conductivity occurs through the grains boundaries.

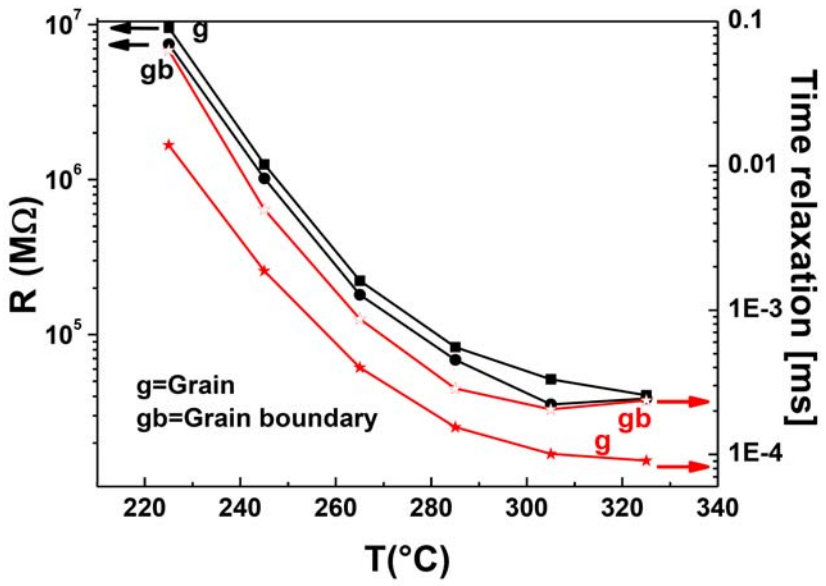

Figure 9. (Color online) Temperature dependence of the resistance and the time relaxation of grain (*g*) and grain boundary (*gb*) in SKN.

It is also natural that relaxation times τ_g and τ_{gb} decrease with temperature. Plots of R_g and R_{gb} versus T yield the Arrhenius law. The conduction of the material and the relaxation activation energy for grains and grains boundaries collected from Figure 9 are given in Table 3. It follows that conduction mechanism is dominated by grains boundaries.

Table 3. Activation energy values for conduction and relaxation of grains and grain-boundaries in SKN paraelectric phase

Grain conduction activation energy, E_g (eV)	**Grain boundary conduction activation energy, E_{gb} (eV)**	**Grain relaxation activation energy, ε_g (eV)**	**Grain boundary relaxation activation energy, ε_{gb} (eV)**
1.411	1.675	1.303	1.796

3.4. Conductivity

Figure 10 illustrates the temperature variation of the AC conductivity at different frequencies of the SKN compound. The Curie temperatures obtained from AC conductivity measurements fit very well with the T_C values found from the curves of the real dielectric constant of SKN. It can be clearly observed that the conductivities at different frequencies increase and appear to be approaching each other at higher temperatures. The change in slope of curve will reflect a change in the conductivity phenomenon in paraelectric and ferroelectric regions.

The activation energy values were calculated by using the Equation (4) for the two regions and are given in Table 4:

$$\sigma_{dc}(T) = \sigma_{dc} \exp(-E/k_B T). \quad (4)$$

From Table 4, the AC conduction activation energies at high frequencies are lower than that at low frequencies. This can be explained by the fact that at low frequencies the conductivity is assured by mobility or transportation over long distances rather than by relaxation/orientation mechanism. The energy required for relaxation/orientation process is higher than that required for mobility of charge carriers over longer distances [28, 29]. The activation energy values obtained at high temperature are attributed to thermal motion of the oxygen vacancies or the formation of association among the oxygen vacancies and residual cations in the grain boundary [30, 31]. The decrease of conductivity in SKN may be caused by the decrease of the oxygen vacancies concentration [32]. The activation energies obtained in the experiments are typical values for an ionic conductor.

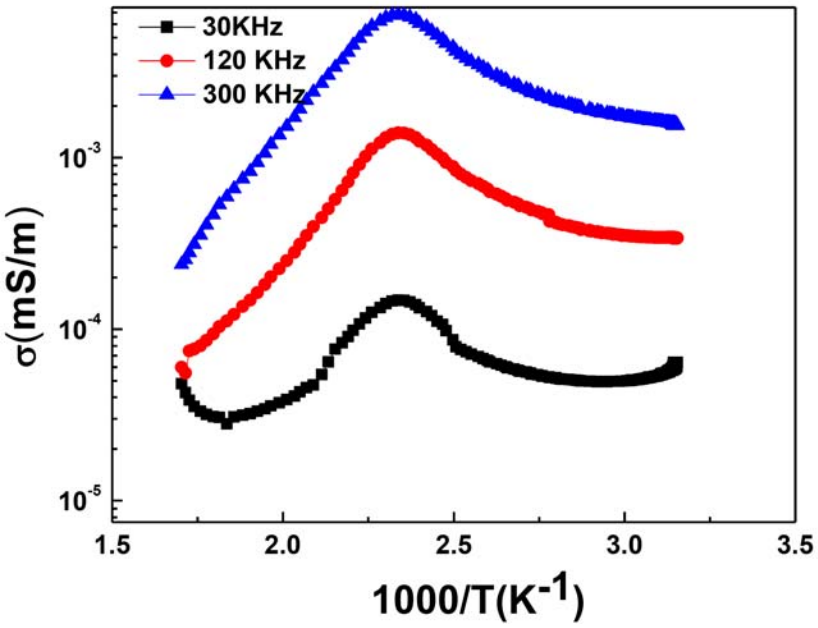

Figure 10. Temperature variation of AC conductivity at different frequencies.

Table 4. Activation energy (eV) values for SKN

Temperature range (ºC)	Activation energy (eV)		
	30KHz	120KHz	300KHz
80-154	0.255	0.238	0.262
154-320	0.394	0.446	0.472

The frequency dependence of AC conductivity (σ_{AC}) for several given temperatures is presented in Figure 11. It shows a plateau at low frequencies and dispersion at high frequencies. The plateau region corresponding to DC conductivity is found to extend to higher frequencies when temperature increases [33]. The frequency, at which the dispersion occurs, also known as hopping frequency, increases with temperature. This behaviour suggests that electrical conductivity takes place through hopping mechanism, which is described by the Jonscher's power law [34]:

$$\sigma_{AC} = \sigma_{DC} + A.(\omega)^n, \quad (5)$$

where σ_{DC} is the direct current conductivity of the sample and ω is the angular frequency of measurement. The n parameter reflects the degree of interaction between mobile ions and the lattices around them, while A is a constant which introduces the polarizability strength.

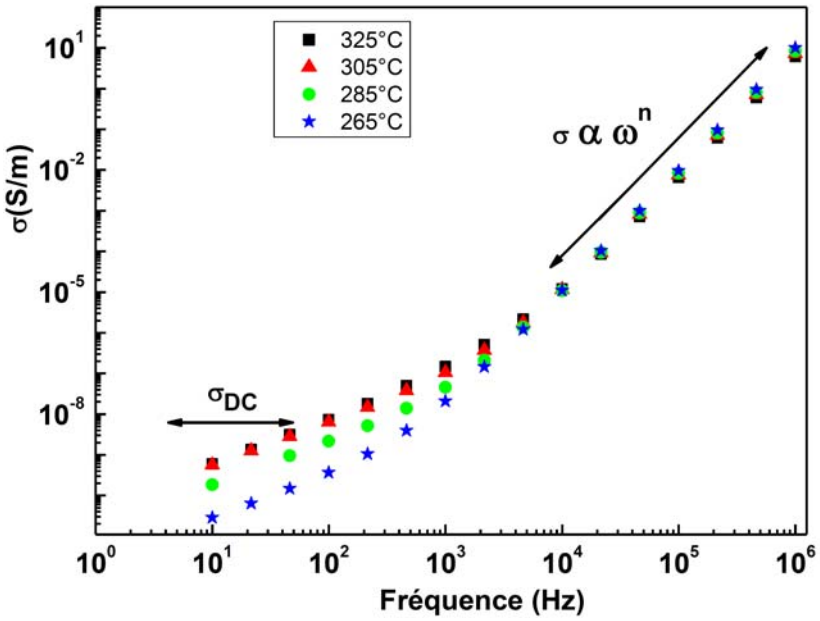

Figure 11. Frequency dependence of the AC conductivity at various temperatures of the SKN compound.

The experimental conductivity curves of the sample are fitted using Equation (5) and the results are depicted in Table 5.

Table 5. Non linear fitting data of SKN compound conductivity

$T(^{\circ}C)$	265	285	305	325
$\sigma_{DC}(10^{-6}Sm^{-1})$	0.22805	0.65531	0.010338	0.014634
$A(10^{-10})$	6.0094	23.818	3.3166	5.8354
n	1.09242	1.35874	1.15678	1.11344

We notice from these values a decreasing tendency of n when temperature increases which is logical regarding the model based on classical hopping of electrons over barrier. In addition and according to Funke [35], when the n value is equal to 1, the hopping motion involves a translational motion with a sudden hopping and when n is greater than 1, the motion involves localized hopping without the species leaving the neighbourhood [36, 37]. The change of tendency in slope takes place at a frequency known as hopping frequency of the polarons (ω_p), which depends on temperature. The AC conductivity follows the Almonde West relation [38] as:

$$\sigma(\omega) = A\omega_p[1 + (\omega/\omega_p)^n], \tag{6}$$

where ω_p is the hopping frequency and n is the Jonscher's constant [39].

The literature [40] have reported that $\sigma_{DC} = A\omega_p$, so the Almonde West relationship becomes:

$$\sigma(\omega) = \sigma_{DC}[1 + (\omega/\omega_p)^n]. \tag{7}$$

The AC conductivity is calculated by using the relationship $\sigma = \omega\varepsilon\varepsilon_0 \tan\delta$. The plateau region of the conductivity at higher frequencies and temperatures may be caused by the space charge. This assumption is reasonable since the space charge effect vanishes at higher temperatures and frequencies. This typical behaviour might be explained by the existence of hopping mechanism between the allowed sites.

4. Conclusion

The new ferroelectric polycrystalline sample of $Sr_2KNb_5O_{15}$ (SKN) of TTB type structure has been prepared by mixed-oxide method. Preliminary structural analysis confirmed the formation of single-phase material in an orthorhombic system at room temperature. A dielectric peak at ~150°C has been observed, suggesting diffuse phase transition.

The parameters characterizing the ferroelectric-paraelectric phase transition in the compound at Curie temperature ~150°C were analysed using the Santos-Eiras phenomenological model. The dielectric properties of the SKN ceramic showed an "incomplete" DPT phase transition around the temperature of the maximum dielectric permittivity (diffusivity $1 < \gamma < 2$) associated with intrinsic disorder of strontium sites and/or the distortions of TTB unit cells.

The dielectric impedance spectroscopy analysis confirms the non-relaxor type behaviour. Reduction of the space-charge polarization and the grain interaction occurs above 150KHz. The dispersion in the high temperature region indicated the localized ionic conductivity.

Study of electrical behaviour using complex impedance analysis (CIS) shows non-Debye poly dispersive behaviour and provides information on the presence of both grain and grain boundary effects in the material; the effect of the material electrode interface is insignificant. The AC conductivity obeys the universal power law.

This new class of lead free ferroelectric SKN is of great interest for green material applications. Crystal growths as well as thin films are in progress.

References

[1] A. Magnéli, Arkiv Kemi 1 (1949), 213.

[2] Y. Gagou, D. Mezzane and N. Aliouane et al., Ferroelectrics 254 (2001), 197.

[3] G. Goodman, J. Am. Ceram. Soc. 36 (1953), 368.

[4] M. Lundberg, M. Sundberg and A. Magnéli, J. Solid State Chem. 44 (1982), 32-40.

[5] X. M. Chen, Y. H. Sun and X. H. Zheng, J. Eur. Ceram. Soc. 23 (2003), 1571.

[6] L. Fang, L. Chen, H. Zhang, C. L. Diao and R. Z. Yuan, Mater. Lett. 58 (2004), 26-54.

[7] R. I. Neurgaonkar, W. F. Hall, J. R. Oliver, W. W. Ho and W. K. Cory, Ferroelectrics 87 (1998), 167.

[8] M. R. Raju and R. N. P. Choudhary, J. Phys. Chem. Solids 64 (2003), 847.

[9] R. R. Neurgaonkar and W. K. Cory, J. Opt. Soc. Am. 3 (1986), 276.

[10] J. Rodrigues-Carvajal, Program Fullprof (2009).

[11] M. El Marssi and Col, J. Appl. Phys. 83 (1998), 5371.

[12] F. De Guerville, M. El Marssi, I. Luk'yanchuk and L. Lahoche, Ferroelectrics 359 (2007), 14.

[13] G. Pascoli, L. Lahoche and I. Luk'yanchuk, Integrated Ferroelectrics 99 (2008), 60.

[14] Y. Amira, Thesis, University Cadi Ayyad (2010), 85.

[15] E. Choukri and Col, Eur. Phys. J. Appl. Phys. 53 (2011), 20901.

[16] K. Sambasiva Rao, P. Murali Krishna, D. Madhava Prasad and Joon Hyung Lee, Int. J. Mod. Phys. B 21 (2007), 931.

[17] T. R. Shrout, L. E. Cross and D. A. Hukin, Ferroelectr. Lett. 44 (1983), 325.

[18] F. G. Jona and G. Shirane, Ferroelectric Crystals, Pergamon, 1962.

[19] D. Viehland, S. J. Jang, L. E. Cross and M. Wuttig, Phys. Rev. B 46 (1992), 8003.

[20] I. A. Santos, D. Garcia and J. A. Eiras, J. Appl. Phys. 93 (2003), 1701-1706.

[21] T. A. Nealon, Ferroelectrics 76 (1987), 377.

[22] M. A. L. Nobre and S. Lanfredi, Mater. Lett. 50 (2001), 322.

[23] M. A. L. Nobre and S. Lanfredi Mater. Lett. 47 (2001), 362.

[24] A. R. James, S. Balaji and S. B. Krupanidhi, Mater. Sci. Eng. B 64 (1999), 149.

[25] J. R. MacDonald and W. B. Johnson, Impedance Spectroscopy, John Wiley & Sons, New York, 2005.

[26] R. El Moznine and Col, J. Phys. D 36 (2003), 330.

[27] A. R. James, S. Balaji and S. B. Krupanidhi, Mater. Sci. Eng. B 64 (1999), 149.

[28] P. B. Macdo, C. T. Moynihan and R. Bose, Phys. Chem. Glasses 13 (1972), 171.

[29] N. Hirose and A. R. West, J. Am. Ceram. Soc. 79 (1996), 1633.

[30] K. Sambasiva Rao, P. Murali Krishna and D. Madhava Prasad, J. Phys. Status Solidi, Wiley-VCH 244 (2007), 2267.

[31] R. C. Buchanan, Ceramic Materials for Electronics, 1992.

[32] R. Gerhardt, J. Phys. Chem. Solids 55 (1994), 1491.

[33] R. Mizaras, M. Takashige, J. Banys, S. Kojima, J. Grigas, Hamazaki, Sin-Ichi and A. Brilingas, J. Phys. Soc. Jpn. 66 (1997), 2881.

[34] A. K. Jonscher, Nature 267 (1977), 673.

[35] K. Funke, Prog. Solid State Chem. 22 (1993), 111-195.

[36] A. Belboukhari and Col, J. Superlattices and Microstructures 71 (2014), 7-22.

[37] S. Sen and R. N. P. Choudhary, Mater. Chem. Phys. 87 (2004), 256.

[38] D. P. Almond, G. K. Duncan and A. R. West, Solid State Ionics 8 (1983), 159-164.

[39] A. K. Jonscher, Nature 267 (1977), 673-679.

[40] K. Prasad, K. Kumari and Col, Mater. Sci. Poland 27 (2009), 373-384.

■